Topologically Linked Protein Rings in the Bacteriophage HK97 Capsid

William R. Wikoff,[1] Lars Liljas,[1,2] Robert L. Duda,[3] Hiro Tsuruta,[4] Roger W. Hendrix,[3] John E. Johnson[1]*

The crystal structure of the double-stranded DNA bacteriophage HK97 mature empty capsid was determined at 3.6 angstrom resolution. The 660 angstrom diameter icosahedral particle contains 420 subunits with a new fold. The final capsid maturation step is an autocatalytic reaction that creates 420 isopeptide bonds between proteins. Each subunit is joined to two of its neighbors by ligation of the side-chain lysine 169 to asparagine 356. This generates 12 pentameric and 60 hexameric rings of covalently joined subunits that loop through each other, creating protein chainmail: topologically linked protein catenanes arranged with icosahedral symmetry. Catenanes have not been previously observed in proteins and provide a stabilization mechanism for the very thin HK97 capsid.

Topological links, or catenanes, are an uncommon feature of molecular architecture. Until recently, only two types were identified: (i) DNA catenanes, in which a circular single strand of DNA forms each link (*1*–*3*), and (ii) organic catenanes, in which each link is formed by a macrocycle (*4*). The first example of a protein catenane, in which a link would be formed by one covalently bonded protein subunit, was recently proposed to form the double-stranded DNA (dsDNA) bacteriophage HK97 capsid (*5*).

Assembly and maturation of tailed dsDNA bacteriophages are highly regulated at the genetic and biochemical levels (*6*). Although there are differences in detail, most phage-assembly pathways have a similar organization. Common features include (i) icosahedral procapsid assembly from several hundred copies of the capsid protein, a separate scaffolding protein, and a portal, required for packaging and release of DNA and tail attachment; (ii) adenosine 5′-triphosphate–driven packaging of phage DNA into the capsid through the portal; (iii) capsid "expansion," in which the subunit interactions are reorganized and the capsid changes shape, increases in volume, and becomes stabilized; and (iv) tail attachment to the portal, which mediates DNA transport into the bacterial cell during infection.

Low-resolution structures of procapsids and mature capsids for dsDNA phages λ (*7*, *8*), HK97 (*9*, *10*), ϕ29 (*11*), and P22 (*12*) have been determined by electron cryomicroscopy (cryo-EM) and image reconstruction. We have determined the first crystal structure of a tailed bacteriophage capsid, HK97, to 3.6 Å resolution. Four stages have been defined in the capsid maturation pathway of HK97, a member of the λ-like bacteriophage family (Fig. 1, A and B). Assembly begins with the *Escherichia coli* GroEL/ES-assisted folding of the gp5 capsid protein and association into hexamers and pentamers. When expressed alone, gp5 assembles into a portal-deficient version of Prohead I. Coexpressing the gp4 protease with gp5 allows wild-type maturational cleavage of gp5, producing Prohead II. Prohead II can then be expanded in vitro into mature Head II (*9*, *13*), containing 420 copies of cleaved gp5 (residues 104 to 385). Prohead II matures to Head II in vivo when dsDNA is packaged into the capsid. Head II is highly stable as a result of the autocatalyzed, isopeptide bond formed between the side chains of Lys^{169} and Asn^{356} in the final maturation step (Fig. 1C) (*13*, *14*). On the basis of the biochemistry, the capsid subunits were proposed to be topologically linked into protein catenanes, or chainmail (*5*). The capsid crystal structure shows how the isopeptide bond is formed between subunits, arranged in topologically linked, covalent circular rings. We term this type of macromolecular assembly protein chainmail because it comprises a three-dimensional fabric of catenated protein circles.

The methods for the growth and data collection of the fragile capsid crystals were reported (*15*). The crystal space group is $P2_1$, with unit cell dimensions a = 581 Å, b = 628 Å, c = 789 Å, β = 89.9°. Determination of the particle orientation and position at 7 Å resolution was described (*16*). The data were subsequently extended to 3.45 Å resolution (*17*), and a total of 22 million reflections (4.8 million unique) were measured on unfrozen crystals. The phasing to 3.6 Å resolution is described in Table 1. Further details of the structure determination will be described elsewhere.

The electron density map was readily interpreted at 3.6 Å, and a model was constructed of the seven gp5 capsid subunits in the icosahedral asymmetric unit (Fig. 2 and 3A) (*18*). Capsid maturation requires the cleavage of 103 residues from the NH_2-terminus of gp5, and thus the sequence numbering of the mature subunit begins with Ser^{104} (Fig. 2). Clearly defined electron density was present for residues 104 to 383; the main chain was visible to Gly^{384}.

HK97 gp5, a new category of virus fold, has no structural similarity to any previously determined capsid protein (Fig. 2). It is a mixed α/β structure (28% α helix; 32% β strand) organized into two compact, spatially distinct domains that are not sequence contiguous. The axial domain A is near the fivefold and quasi sixfold symmetry axes, and the peripheral domain P, plus extensions (N-arm and E-loop), fill the region between adjacent quasi or icosahedral threefold axes (Fig. 3A).

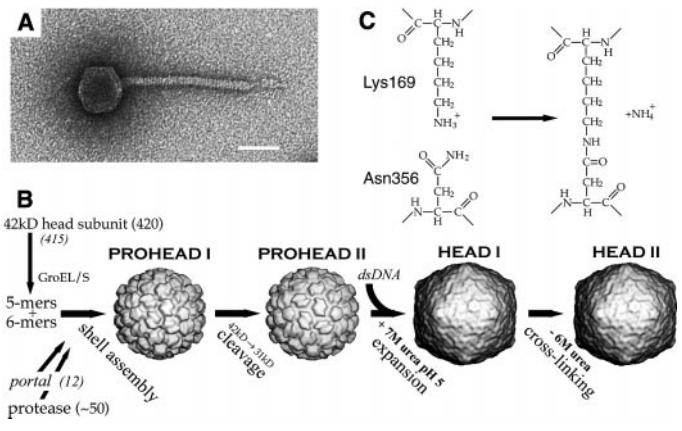

Fig. 1. HK97 assembly and maturation. (**A**) Negatively stained electron micrograph of a mature dsDNA-filled capsid, with noncontractile tail and accessory proteins. (**B**) Steps in capsid assembly and maturation (see text; in vitro conditions are in bold, and in vivo conditions or components that differ from the in vitro conditions are in italic) (*9*). (**C**) Chemistry of the cross-linking reaction.

[1]Department of Molecular Biology, Scripps Research Institute, 10550 North Torrey Pines Road, La Jolla, CA 92037, USA. [2]University of Uppsala, Biomedical Center, Department of Cell and Molecular Biology, Box 596, S-751 24 Uppsala, Sweden. [3]Pittsburgh Bacteriophage Institute and Department of Biological Sciences, University of Pittsburgh, Pittsburgh, PA 15260, USA. [4]Stanford Synchrotron Radiation Laboratory, Stanford University, Post Office Box 4349, Stanford, CA 94309, USA.

*To whom correspondence should be addressed. E-mail: jackj@scripps.edu

Together, domains A and P alone form an L-shaped monomer. The core of the 48 Å long domain A is a four-stranded antiparallel β sheet packed against helix α5 and protrudes slightly from the capsid surface. Strand βK of this sheet forms the gp5 COOH-terminus on the capsid exterior. A 21-residue insertion between α6 and βF forms, with its symmetry mates, an interior annulus at the pentamer and hexamer axes (Figs. 2 and 3A). Domain P spans the quasi threefold and twofold axes of the particle and is, without the extensions, ~63 Å long and slightly smaller in radius than domain A. Domain P comprises a 43 Å long α helix (α3′/3″), packed against a three-stranded antiparallel β sheet. There is an unusual eight–amino acid loop (α3′-α3″ loop) inserted within this helix near its COOH-terminal end and extending 15 Å outward to the capsid surface from the center of the helix axis (Fig. 2). Three glycine residues provide folding flexibility, but the loop is stabilized by a salt bridge and hydrogen bonding, and the electron density is well resolved and therefore not exceptionally mobile. The α3 helix continues for one additional turn (α3″) past the loop.

The unusual form, organization, and function of the subunits derive from the N-arm and E-loop and their acrobatic quaternary associations. The N-arm is formed by residues 104 to 132 (Fig. 2) and extends 67Å from the monomer core. The conformation is extended, and the polypeptide displays several changes in direction, facilitated by three proline residues. Most of the N-arm runs underneath an adjoining subunit on the capsid interior surface, but the NH_2-terminus is on the capsid exterior surface and contacts two other symmetry-related monomers (Fig. 4A). The E-loop (residues 148 to 181), following the N-arm in sequence, is a 52-Å-long, two-stranded antiparallel sheet connected by a turn. It spans the quasi twofold and threefold axes and contains Lys^{169}, one of the two residues forming the isopeptide bond between subunits, and contacts two other symmetry-related monomers (Fig. 3, A and B).

The HK97 capsid has the symmetry and shape of an icosahedron, with a maximum diameter of 659 Å along the fivefold axes (Fig. 3B). The thickness of the shell is only 18 Å or less, giving the empty particle the appearance of an icosahedral balloon (Fig. 3C). The HK97 capsid is thinner than eukaryotic viruses constructed with a β barrel, which are typically 40 Å or more thick. The capsid is constructed from pentamers and hexamers, with seven unique copies of the

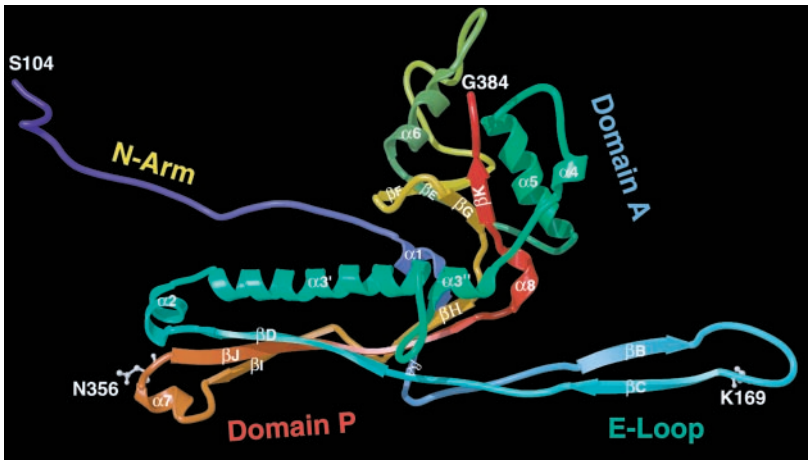

Fig. 2. Structure of one gp5 subunit, color ramped from the NH_2-terminus (violet) to the COOH-terminus (red) (label colors correspond to Fig. 3A domain colors). The Head II NH_2-terminus becomes Ser^{104} by maturational proteolysis in the Prohead I to II transition. The subunit is organized into A and P domains, plus the extended N-arm (violet) and E-loop (cyan). Lys^{169}, on the E-loop, forms an isopeptide bond with Asn^{356} on a neighboring subunit.

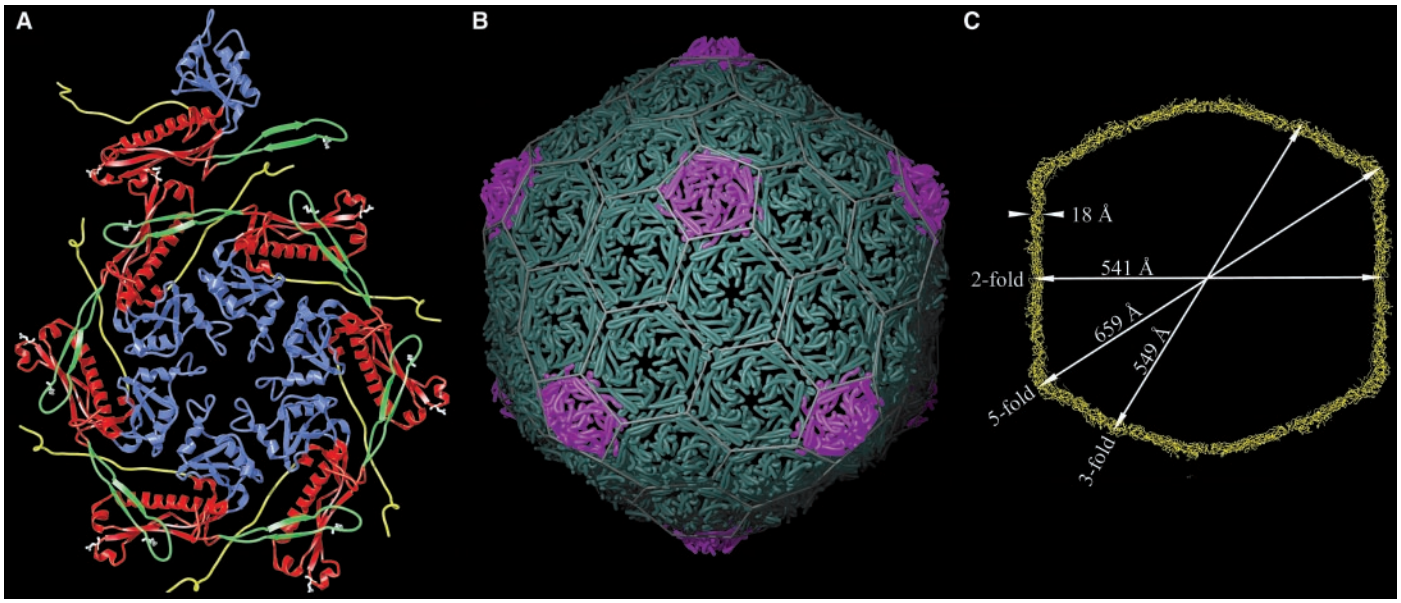

Fig. 3. Capsid organization. (**A**) The capsid asymmetric unit (A domain: blue; P domain: red; N-arm: yellow; E-loop: green). The capsid is a $T = 7$ arrangement of 420 subunits, organized into hexamers (one shown) and pentamers (one pentamer subunit is shown). The subunits wrap around each other in an intricate arrangement. Cross-links cannot form between subunits within the asymmetric unit, because the cross-linking residues (Lys^{169} and Asn^{356} in white) are not in close proximity. (**B**) The complete capsid from the particle exterior (each subunit backbone is a smoothed tube). The hexamers (green) are flat, with most of the particle curvature at the concave pentamer (magenta), producing the distinctive icosahedral capsid shape. A $T = 7$ cage (gray) indicates the quasi symmetry axes. The pentagon and hexagon vertices are icosahedral or quasi threefold axes, with icosahedral or quasi twofold axes equidistant between them. (**C**) Cross section through the unusually thin empty capsid, which despite its large size (659 Å along fivefold), is only 18 Å thick. Icosahedral symmetry axes are indicated.

polypeptide chain in the icosahedral asymmetric unit arranged with $T = 7$ quasi symmetry (Fig. 4B), an arrangement not previously observed in a high-resolution structure. The hexamers display high-fidelity sixfold symmetry, with subunit backbone conformations that are similar except for the hexamer/pentamer annulus and N-arm and E-loop. An icosahedron organized with a $T = 7$ lattice is enantiomorphic; the capsid hand, determined from the crystal structure, is *levo*. The closest example to this quasi symmetry in a crystal structure is the papovavirus capsid, arranged on a $T = 7$ *dextro* lattice, but with pentamers substituted in the hexavalent lattice positions (*19*). HK97 contains nine arginine residues per subunit on the interior particle surface that may interact with the adjacent dsDNA to neutralize its negative charge (*20*).

Subunit interactions are extensive; each subunit contacts four others within its own hexamer or pentamer, making additional nonbonded contacts with subunits beyond the morphological units, and finally forming covalent bonds to two subunits from two different hexamers or pentamers (Fig. 3, A and B). There is a remarkable shape complementarity between the hexamer and pentamer subunits, particularly in contacts between adjacent A domains. Subunit interactions are stabilized by a typical combination of van der Waals contacts, hydrogen bonds, and salt bridges (*21*), plus the unusual isopeptide bonds.

The hexamers are nearly planar, whereas the pentamers are concave, thereby introducing capsid curvature (Fig. 3, B and C). These differences in dihedral angles between subunits appear to arise from small variations in side-chain interactions. The N-arm and E-loop conformations, leveraged by their length, display exaggerated differences between hexamers and pentamers, to accommodate the surface curvature. We speculate that conformational differences in the N-arm and E-loop accommodate the particle structure, rather than functioning as a conformational switch regulating particle assembly. The mature capsid subunits are intertwined so extensively that the need to first construct a procapsid precursor followed by maturation in discrete steps is easily rationalized.

Each subunit of the HK97 capsid is covalently bonded to two neighboring subunits through the ligation of a Lys^{169} side chain to Asn^{356} via an isopeptide bond. The bond organization explains why the mature HK97 particles are extraordinarily stable and cannot be disassembled to enter an SDS gel (*14*) without protease treatment (*5*). Biochemical analysis was used to identify the bond-forming residues, and protein chainmail was proposed to explain the unusual biochemistry. Duda (*5*) proposed that cross-links were formed between subunits of the pentamer and hexamer within the capsomers, and that polypeptide chains from neighboring capsomers were intertwined to hook subunits from adjoining morphological units, thereby constructing a topological link from each subunit. The structure of the capsid confirms the existence of covalent protein circles and their topological interlinking as deduced from the biochemical experiments. However, the structure is different from what was originally envisaged (*5*), as described below.

Protein chainmail has three levels of organization: (i) 420 isopeptide bonds between Lys^{169} and Asn^{356} on neighboring subunits (ii) join monomers together into covalent rings (meta-hexamers and pentamers), (iii) which are organized topologically into catenated links by capsid icosahedral symmetry. These three components together create capsid chainmail (Fig. 4).

Individual subunits are cross-linked into hexameric and pentameric rings of subunits, which we call metahexamers and pentamers, because these covalent subunit rings encircle, rather than form, the hexamer or icosahedral pentamer, from which the capsid assembles (e.g., Fig. 4, A an B) (*22*). The symmetry of the metahexamer approximates the quasi sixfold symmetry of the hexamer that it encircles. When the icosahedral symmetry is applied to the metahexamer or pentamer, the

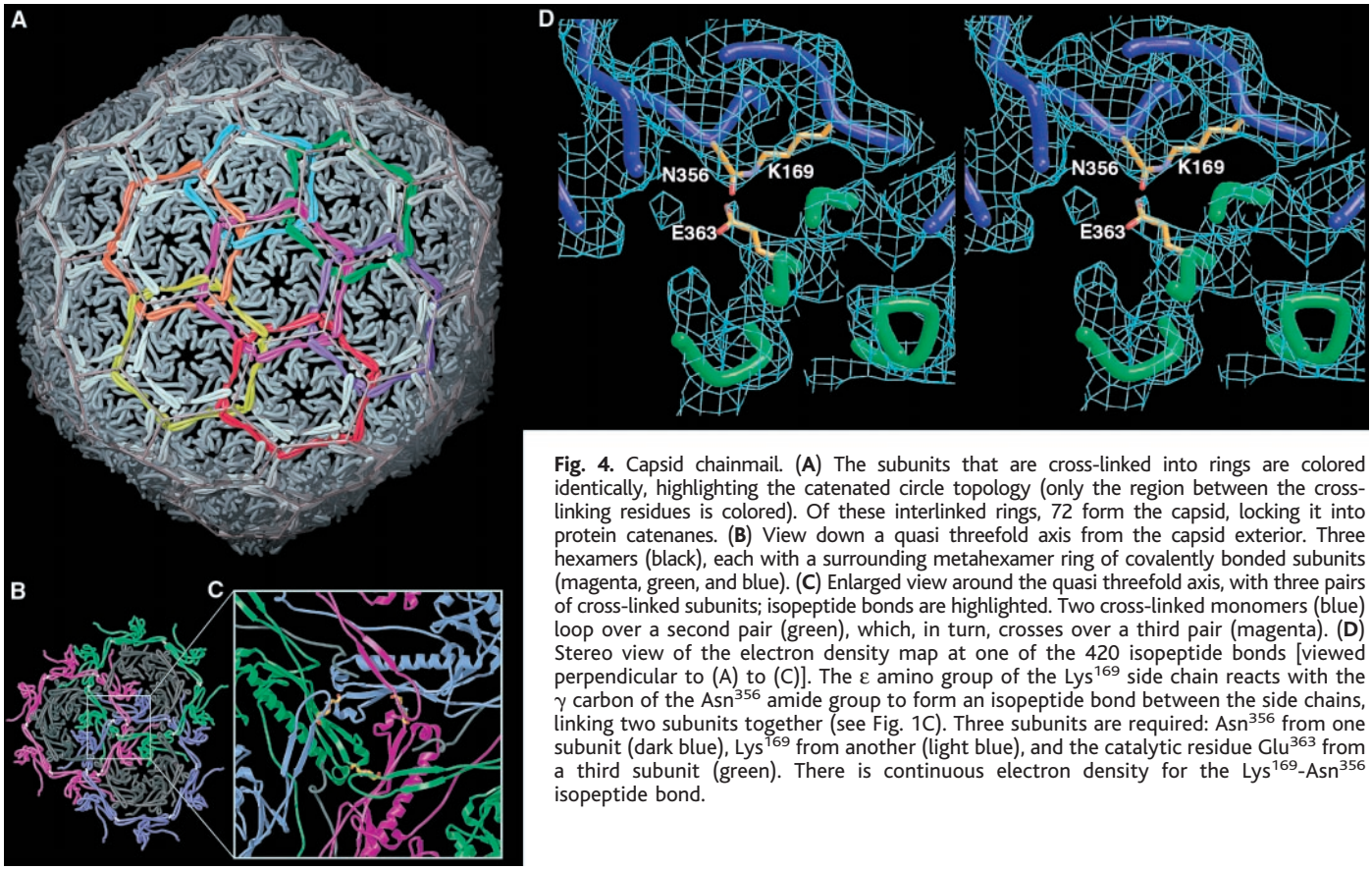

Fig. 4. Capsid chainmail. (**A**) The subunits that are cross-linked into rings are colored identically, highlighting the catenated circle topology (only the region between the cross-linking residues is colored). Of these interlinked rings, 72 form the capsid, locking it into protein catenanes. (**B**) View down a quasi threefold axis from the capsid exterior. Three hexamers (black), each with a surrounding metahexamer ring of covalently bonded subunits (magenta, green, and blue). (**C**) Enlarged view around the quasi threefold axis, with three pairs of cross-linked subunits; isopeptide bonds are highlighted. Two cross-linked monomers (blue) loop over a second pair (green), which, in turn, crosses over a third pair (magenta). (**D**) Stereo view of the electron density map at one of the 420 isopeptide bonds [viewed perpendicular to (A) to (C)]. The ε amino group of the Lys^{169} side chain reacts with the γ carbon of the Asn^{356} amide group to form an isopeptide bond between the side chains, linking two subunits together (see Fig. 1C). Three subunits are required: Asn^{356} from one subunit (dark blue), Lys^{169} from another (light blue), and the catalytic residue Glu^{363} from a third subunit (green). There is continuous electron density for the Lys^{169}-Asn^{356} isopeptide bond.

adjoining symmetry-related rings become topologically linked. For example, three metahexamers are interlocked around each threefold axis (Fig. 4B in magenta, green, and blue). Each pair of these metahexamers is related by twofold symmetry (magenta and green); one meta-hexamer (magenta) loops above and through the other (green), maintaining the icosahedral twofold symmetry. The same relation holds between the other two pairs of rings (blue:green and blue:magenta) related by threefold symmetry. Thus, the linking is perpetuated throughout the capsid and is an elegant outcome of icosahedral symmetry. A total of 72 metahexamer/pentamer rings form the capsid: 60 metahexamers and 12 metapentamers.

Table 1. Structure determination. Data statistics are to 3.45 Å resolution, and the current phases were determined to 3.6 Å resolution. Low-resolution reflections were measured and included in the data set between 200 and 16 Å resolution. Collection of low-resolution x-ray data (SSRL beam line 4-2) was crucial to overlap with the low-resolution cryo-EM phasing model (maximum resolution, 25 Å). They were merged with two moderate-resolution data sets (CHESS beam line F-1) and two 3.6 Å resolution data sets (APS BioCARS beamline 14BM-C). The data were processed, scaled, and post-refined with the programs DENZO, SCALEPACK (*41*), and AGROVATA (*42*). The structure determination used molecular replacement averaging and phase extension, with the program packages RAVE (*43*) and CCP4 (*42*). One virus particle per crystallographic asymmetric unit provides 60-fold noncrystallographic symmetry. A cryo-EM reconstruction of HK97 Head II was used to build a low-resolution phasing model with scattering centers placed on a uniform grid within the envelope (*9*). After adjusting the radial scale of the model based on the x-ray structure factors, phases were calculated between 200 and 50 Å resolution and combined with the measured x-ray amplitudes. Real-space averaging was initiated between 200 and 50 Å resolution, and phases were extended one reciprocal lattice step at a time with five cycles of averaging at each step. The interpretability of the final map was improved by applying an artificial *B* factor of −40 Å^2 to the structure factors to up-weight the higher resolution terms.

Space group*	$P2_1$
Unit cell	a = 581.22, b = 628.35, c = 789.45, β = 89.94
Number of images	760
D_{min} (Å)	3.45
Measured reflections	21,863,976
Possible unique reflections	7,347,473
Measured unique reflections	4,800,765
Completeness (%)†	63.0
Overall R_{merge} (%)‡	16.0
$\langle I/\sigma(I)\rangle$	9.6
Minimum partiality accepted	0.5
Averaging *R* factor§	0.32
Correlation coefficient‖	84.8

*Packing and systematic absences (0*k*0, *k* = even) indicated space group $P2_1$, confirmed with the self-rotation function. †Completeness was 34.6% between 3.65 and 3.58 Å resolution. ‡At 4.0 Å resolution, R_{merge} = 38.5%. §$R = \sum_{hkl}(|F_{obs}| - k|F_{calc}|)/\sum_{hkl}|F_{obs}|$. ‖$CC = \sum_{hkl}(|F_{obs}| - \langle|F_{obs}|\rangle)(|F_{calc}| - \langle|F_{calc}|\rangle)/(\sum_{hkl}(|F_{obs}| - \langle F_{obs}\rangle)^2 \sum_{hkl}(|F_{calc}| - \langle|F_{calc}|\rangle)^2)^{1/2}$.

The isopeptide bonds are close to the threefold symmetry axes (Fig. 4C), around which nine subunits interact in a nexus of quaternary interactions. Three P domains, three N-arms, and three E-loops, from nine different subunits, interact within a small volume (*23*). The isopeptide bond between Lys^{169} and Asn^{356} side chains, linking two subunits, is clearly visible in the density for all seven subunits (shown for one in Fig. 4D). The Glu^{363} carboxyl from a third subunit is hydrogen-bonded to the carbonyl oxygen of the isopeptide (Fig. 4D). The reaction that forms this bond is autocatalytic and is the final step of capsid maturation. Cross-linking can be abolished by mutating Lys^{169} to Tyr, which assembles, cleaves, and matures to Head I, but does not cross-link (*24*). Cross-linking can also be abolished by mutation of Glu^{363} to Ala, resulting in normal assembly and maturation, but preventing cross-linking (*25*). This suggests that Glu^{363} is required for the catalytic mechanism. Protein chainmail completely explains the complex biochemical data on the unusual HK97 capsid stability.

There are striking similarities in assembly and maturation among the tailed dsDNA phages. Cryo-EM reconstructions of HK97 (*9*), P22 (*12*), lambda (*7*, *8*), and even the animal virus herpes (*26*), show that the hexamers are asymmetric and protrude from the procapsid but flatten out and adopt sixfold symmetry in the mature capsid. Many mature phage capsids share features including the icosahedral shape, very thin shells, and *levo* parity of the T = 7 quasi symmetry (*6*, *27*–*29*). A cryo-EM reconstruction of the gpD$^-$ phage lambda capsid (*7*) appears strikingly similar to HK97 Head II at low resolution. The similarities suggest a deeper structural homology between phage capsids in different taxonomic groups, even though their sequence similarity is very low. Only additional high-resolution structures will reveal whether the common features are the result of a remarkable convergence of function or are so widely diverged that only similarity in structure and function are detectable. The HK97 capsid protein has one clear homolog, the capsid protein of the *Pseudomonas* phage D3, which also forms cross-links (*30*). They have 41% sequence identity, and the cross-linking Lys^{169} and Asn^{356} residues and the putative catalytic residue, E363, are conserved (*31*).

High-resolution structures of phage capsids with single-stranded RNA (ssRNA) and ssDNA genomes were determined previously. The ssDNA phage ϕX174 capsid (*32*) and the dsDNA phage PRD1 hexon (*33*) both display the common β-sandwich folds of eukaryotic viruses. ssRNA phages, such as MS2 (*34*), have a novel fold compared with eukaryotic ssRNA viruses, suggesting an evolutionary path independent from that of the canonical capsid β sandwich. The HK97 capsid bears no resemblance to either of these folds, suggesting a separate evolutionary path for tailed bacteriophage capsids.

HK97 is the first example of a protein catenane. Two types of molecular catenanes have been described: DNA catenanes (including Borromean rings) (*1*–*3*) and synthetic organic catenanes (*4*). The arrangement of chainmail links in the HK97 capsid can be described in topological terms. Each pair of metahexamer and pentamer links that is related by an icosahedral or quasi twofold axis is in a left-handed antiparallel arrangement (*35*). In the set of three interlocked rings that associate around the threefold axis, every pair of two rings is linked together, and thus the topology is not a classic Borromean ring structure.

Most plant and animal viruses must balance capsid stability for nucleic acid protection with the need to disassemble during infection. Tailed bacteriophages circumvent disassembly by injecting dsDNA directly into the bacterial cell through the tail. Most phage probably do not form cross-links, but may stabilize the capsid by functionally analogous means, such as accessory protein addition at the threefold axes (*7*, *36*). Considering the severe environments from which phage have been isolated, increased capsid stability may provide an evolutionary advantage. Decreased stability in the absence of HK97 cross-linking was demonstrated with a mutant (Lys^{169}→Tyr) that abolishes isopeptide bonding, but produces otherwise normal-appearing capsids (*5*, *24*). This mutant protein failed to form infectious particles in a complementation assay (*25*); the cross-links may have replaced other preexisting stabilizing elements during evolution.

A linear cross-linking of proteins by means of isopeptide bonds occurs in fibrin clotting, where the biological role is to provide increased clot stability (*37*). Fibrin subunits cross-link by Lys-Gln side-chain ligation, catalyzed by a separate transglutaminase enzyme containing a cysteine protease-like active site (*38*). Although the Lys-Asn isopeptide in HK97 is chemically similar to fibrin, no mechanistic similarity is apparent from the structure. HK97 may be a unique example of a transamidation reaction where isopeptide bonding is autocatalytic, and is unusual in ligating Lys to Asn, rather than Gln.

Asparagine side chains can deaminate or cleave through a cyclic imide intermediate formed by a nucleophilic attack of the main-chain carbonyl carbon by the asparagine side-

chain nitrogen (*39*). This suggests a mechanism for HK97 cross-linking, in which Glu^{363} increases the nucleophilicity of the Asn^{356} nitrogen, and a succinimide intermediate is followed by ligation, rather than cleavage. Although protein cross-links are not known to form by cyclic imide intermediates, peptides have been shown to ligate by this mechanism (*40*). Alternatively, formation of a Schiff-base intermediate involving Lys^{169} could be enhanced by deprotonation of the Lys^{169} ε-amino group by Glu^{363}.

The complexity of the HK97 capsid structure is striking, but represents only the final stage of maturation. Capsid assembly and maturation require a regulatory process of commensurate complexity to the final assembly product, and the goal is to understand this process in molecular detail. Prohead II, round in shape and extensively corrugated, with hexamers skewed into a dimer of trimers, is radically reorganized during maturation. Maturation involves an "ironing out" of these corrugations and an unskewing of the hexamers, producing the larger size, icosahedral shape, and smooth surface of Head II. Structures of three transitory intermediates between Prohead II and Head II, staging posts on the pathway of capsid reorganization, were recently determined by cryo-EM reconstruction (*10*). The stage is now set to understand HK97 morphogenesis in chemical detail.

References and Notes

1. O. Sundin and A. Varshavsky, *Cell* **21**, 103 (1980).
2. J. Chen, C. A. Rauch, J. H. White, P. T. Englund, N. R. Cozzarelli, *Cell* **80**, 61 (1995).
3. N. C. Seeman, *Annu. Rev. Biophys. Biomol. Struct.* **27**, 225 (1998).
4. J. P. Sauvage and C. Dietrich-Buchecker, Eds., *Molecular Catenanes, Rotaxanes and Knots* (Wiley-VCH, New York, 1999).
5. R. L. Duda, *Cell* **94**, 55 (1998).
6. S. Casjens and R. Hendrix, in *The Bacteriophages*, R. Calendar, Ed. (Plenum, New York, 1988), p. 15.
7. T. Dokland and H. Murialdo, *J. Mol. Biol.* **233**, 682 (1993).
8. F. Yang, *et al.*, *Nature Struct. Biol.* **7**, 230 (2000).
9. J. F. Conway, R. L. Duda, N. Cheng, R. W. Hendrix, A. C. Steven, *J. Mol. Biol.* **253**, 86 (1995).
10. R. Lata *et al.*, *Cell* **100**, 253 (2000).
11. Y. Tao *et al.*, *Cell* **95**, 431 (1998).
12. P. A. Thuman-Commike *et al.*, *J. Mol. Biol.* **260**, 85 (1996).
13. R. L. Duda *et al.*, *J. Mol. Biol.* **247**, 618 (1995).
14. M. P. Popa, T. A. McKelvey, J. Hempel, R. W. Hendrix, *J. Virol.* **65**, 3227 (1991).
15. W. R. Wikoff, R. L. Duda, R. W. Hendrix, J. E. Johnson, *Virology* **243**, 113 (1998).
16. _____, *Acta Crystallogr. D* **55**, 763 (1999).
17. W. R. Wikoff, W. Schildkamp, J. E. Johnson, *Acta Crystallogr. D* **56**, 890 (2000).
18. The model was built with the program O [T. A. Jones, J. Y. Zou, S. W. Cowan, Kjeldgaard, *Acta Crystallogr. A* **47**, 110 (1991)]. The programs MOLSCRIPT [P. J. Kraulis, *J. Appl. Crystallogr.* **24**, 946 (1991)] and BOBSCRIPT [R. M. Esnouf, *J. Mol. Graphics Modelling* **15**, 132 (1997)] were used with Raster3D [E. A. Merritt and D. J. Bacon, *Methods Enzymol.* **277**, 505 (1997)] for Figs. 2 to 4.
19. R. C. Liddington *et al.*, *Nature* **354**, 278 (1991).
20. Residues Arg-131, 135, 142, 194, 294, 338, 347, 365, and 372 are accessible to the interior capsid surface.
21. Domain A helices α5 and α6 from adjoining subunits pack together in an antiparallel arrangement. A cluster of hydrophobic residues form a pocket at the subunit interface, into which Trp^{309} from a neighboring subunit fits. Around annuli at the hexamer and pentamer axes, the subunit interactions are stabilized by symmetric hydrogen bond networks. The subunits form even more intricate associations around the quasi two- and threefold axes.
22. Z. Xie and R. W. Hendrix, *J. Mol. Biol.* **253**, 74 (1995).
23. The N-arm interacts with the E-loops from two different subunits at the quasi threefold axis. The face of the P domain three-stranded β sheet forms a concave pocket into which the knoblike end of a quasi threefold-related domain P fits. Arg^{194}, on the α2 helix knob, and Glu^{344}, in the pocket on strand βI, form a salt bridge, 3.5 Å from the putative catalytic Glu^{363} carboxylate.
24. R. L. Duda, K. Martincic, R. W. Hendrix, *J. Mol. Biol.* **247**, 636 (1995).
25. W. R. Wikoff *et al.*, unpublished results.
26. B. L. Trus *et al.*, *J. Mol. Biol.* **263**, 447 (1996).
27. A. C. Steven, P. Serwer, M. E. Bisher, B. L. Trus, *Virology* **124**, 109 (1983).
28. R. C. Williams and K. E. Richards, *J. Mol. Biol.* **88**, 547 (1974).
29. W. C. Earnshaw, *J. Mol. Biol.* **131**, 14 (1979).
30. Z. A. Gilakjan and A. M. Kropinski, *J. Bacteriol.* **181**, 7221 (1999).
31. W. R. Wikoff *et al.*, data not shown.
32. R. McKenna *et al.*, *Nature* **355**, 137 (1992).
33. S. D. Benson, J. K. Bamford, D. H. Bamford, R. M. Burnett, *Cell* **98**, 825 (1999).
34. K. Valegard, L. Liljas, K. Fridborg, T. Unge, *Nature* **345**, 36 (1990).
35. J. H. White and N. R. Cozzarelli, *Proc. Natl. Acad. Sci. U.S.A.* **81**, 3322 (1984).
36. A. C. Steven, H. L. Greenstone, F. P. Booy, L. W. Black, P. D. Ross, *J. Mol. Biol.* **228**, 870 (1992).
37. C. S. Greenberg, P. J. Birckbichler, R. H. Rice, *FASEB J.* **5**, 3071 (1991).
38. V. C. Yee *et al.*, *Proc. Natl. Acad. Sci. U.S.A.* **91**, 7296 (1994).
39. T. Geiger and S. Clarke, *J. Biol. Chem.* **262**, 785 (1987).
40. R. Lura and V. Schirch, *Biochemistry* **27**, 7671 (1988).
41. Z. Otwinowski and W. Minor, in *Methods in Enzymology*, Part A, *Macromolecular Crystallography*, C. W. J. Carter and R. M. Sweet, Eds. (Academic Press, New York, 1997), vol. 276, p. 307.
42. Collaborative Computational Project Number 4, *Acta Crystallogr. D* **50**, 760 (1994).
43. G. J. Kleywegt and A. T. Jones, in *From First Map to Final Model*, S. Bailey, R. Hubbard, D. Waller, Eds. (Science and Engineering Research Council, Daresbury Laboratory, Warrington, UK, 1994), p. 59.

44. We thank J. Conway, N. Cheng, and A. Steven for providing the HK97 capsid cryo-EM reconstruction. Assistance of the Cornell High Energy Synchrotron Source (CHESS), Advanced Photon Source (APS), and Stanford Synchrotron Radiation Laboratory (SSRL) staffs is gratefully acknowledged. Supported by NIH grants AI40101 (J.E.J.) and GM47795 (R.W.H.). Coordinates for the crystal structure of the bacteriophage HK97 capsid have been deposited with the Protein Data Bank (accession no. 1FH6).

26 April 2000; accepted 28 July 2000

Activation of the DNA Replication Checkpoint Through RNA Synthesis by Primase

W. Matthew Michael,[1,2]* Robert Ott,[3] Ellen Fanning,[3] John Newport[1]

When DNA replication is inhibited during the synthesis (S) phase of the cell cycle, a signaling pathway (checkpoint) is activated that serves to prevent mitosis from initiating before completion of replication. This replication checkpoint acts by down-regulating the activity of the mitotic inducer cdc2-cyclin B. Here, we report the relation between chromatin structure and induction of the replication checkpoint. Chromatin was competent to initiate a checkpoint response only after the DNA was unwound and DNA polymerase α had been loaded. Checkpoint induction did not require new DNA synthesis on the unwound template strand but did require RNA primer synthesis by primase. These findings identify the RNA portion of the primer as an important component of the signal that activates the replication checkpoint.

The DNA replication checkpoint prevents mitosis if DNA replication is either ongoing or blocked during S phase (*1*). Precisely which structural elements of replicating DNA serve to activate the checkpoint is currently not known. To address this issue, we have used *Xenopus* extracts, a biochemically tractable system, to define the replication structure(s) that activates the replication checkpoint.

Upon checkpoint induction, the Chk1 protein kinase is phosphorylated and activated (*2*). Activated Chk1 phosphorylates the Cdc25 protein phosphatase, resulting in negative regulation of Cdc25 and a subsequent delay on entrance into mitosis (*3*). In *Xenopus*, the Chk1 pathway functions in the replication checkpoint (*4*). Induction of the replication checkpoint in egg extracts induces Chk1 phosphorylation, and removal of Chk1 from extracts attenuates replication checkpoint control of mitosis.

Checkpoint-induced phosphorylation of

[1]Department of Biology, University of California, San Diego, La Jolla, CA 92093–0349, USA. [2]Department of Molecular and Cellular Biology, Harvard University, Cambridge, MA 02138, USA. [3]Department of Molecular Biology, Vanderbilt University, Nashville, TN 37235, USA.

*To whom correspondence should be addressed. E-mail: matt@mcb.harvard.edu